

## Molarity Dependent Structural and Dielectric Behavior of Calcium Titanate Ceramics

Muhammad Usama Khan<sup>1,2</sup>, Nawishta Jabeen<sup>1</sup>, Sajid Nawaz<sup>3</sup>, Qaiser Shahzad<sup>1</sup>, Muhammad Awais Anwar<sup>1</sup>, Saira Riaz<sup>2</sup>, Muhammad Imran<sup>2</sup>, Shahzad Naseem<sup>2</sup>, Ahmad Hussain<sup>1,\*</sup>

<sup>1</sup>Department of Physics, The University of Lahore, Sub-campus Sargodha, 40100, Pakistan

<sup>2</sup>Centre of Excellence in Solid State Physics, University of the Punjab, Lahore, 54590, Pakistan

<sup>3</sup>School of Mechanical Engineering, EME College, National University of Science and Technology, Rawalpindi, 4600, Pakistan

\*Corresponding Author: Dr. Ahmad Hussain

**ABSTRACT :** Calcium titanate ( $\text{CaTiO}_3$ ) is most studied perovskite material due to its innovative dielectric properties. In this work, the effect of molarity on structural, dielectric and impedance spectroscopic has been observed. X-ray diffraction analysis has confirmed the orthorhombic crystal structure of the samples. The frequency dependent dielectric and impedance performed in a wide frequency range (20Hz–20MHz) at room temperature. The behavior of dielectric parameters is studied by using Maxwell-Wagner's model and Koop's theory. The variation of AC conductivity with frequency obeys Jonscher's power law. The variation of frequency exponent 's' values (0.385 to 0.802) show that conduction mechanism, which arises due to polaron hopping. Electroactive regions are investigated with the help of Nyquist plot. Frequency-dependent Nyquist plot describes the effect of grain boundaries in all samples of  $\text{CaTiO}_3$ .

**KEYWORDS** Perovskite,  $\text{CaTiO}_3$ , Dielectric, Impedance

Date of Submission: 21-08-2021

Date of acceptance: 05-09-2021

### I. INTRODUCTION

Perovskite materials have incredible interest for scientists in ongoing decades for attractive ferroelectric, pyroelectric, dielectric, piezoelectric, catalytic properties [1-3]. These materials possess significant importance in potential technological applications of bio-sensing devices, catalysis, superconductors, non-linear optics, fuel cells, detectors, storage memories, multilayer ceramic capacitors (MLCC) and pyroelectric detectors [4-7]. Perovskite materials with the general relation of  $\text{ABO}_3$ , A-site and B-sites elements play vital role to affect/enhance the properties of the materials [8-10].

For environmental alertness, now Pb-free perovskite ceramics are under examination for electronics applications [11].  $\text{CaTiO}_3$  is one of the most promising ferroelectric perovskite material. Below 1380K, it shows the orthorhombic structure with space group  $Pbnm$ . When phase transition occurs between 1380 to 1500K the orthorhombic structure converts into tetragonal structure with space group  $14/mcm$ . The cubic phase arises above 1500K with space group  $Pm3m$ . The bending is created in  $\text{CaTiO}_3$  structure because of arranged  $\text{TiO}_6$  octahedral [12, 13].  $\text{CaTiO}_3$  is unique among all perovskite titanates because of its high dielectric constant, low dielectric loss, good photocatalytic activity, wide band gap 3.4-3.9eV, luminescent, good thermal and chemical stable behaviors [14, 15]. Han *et al.* [8] reported the effect of three different preparation methods on photocatalytic activity of  $\text{CaTiO}_3$ . Hosseini [16] investigated the effect of different chemicals on photocatalytic activity and on morphology of  $\text{CaTiO}_3$  nanoparticles. Cesconeto *et al.* [13] studied the effect of calcined  $\text{CaTiO}_3$  on structural, morphological and photocatalytic properties. The calcined temperature range is 300-900°C. Wong *et al.* [17] studied the effect of sintering on dielectric, impedance and modulus behaviour of  $\text{CaTiO}_3$  at temperature 1240°C. Cibor *et al.* [18] studied the effect of annealing in temperature range of 530-1170°C on dielectric properties of  $\text{CaTiO}_3$  synthesized by plasma spray technology. Solid state method for the fabrication of  $\text{CaTiO}_3$  possesses several drawbacks, like impurities, non-uniformity and irregular surface morphologies [19,20]. To overcome these drawbacks, various methods such as, wet chemical method, co-precipitation [21], combustion

[22], polymeric precursor [23], organic-inorganic [24], were followed by several researchers. Among various techniques sol-gel has gained attention due to resulting remarkable properties, good stoichiometric control, low temperature handling, high homogeneity, non-vacuum, simple handling, high purity, producing uniform thin films when dip coating is used [25,26]. Herein, this research work is quite unique because no researcher reported calcium titanate ceramic with such variation of molarity by sol-gel method.

## II. EXPERIMENTAL DETAILS

All reagents, Tetra-butyl Titanate [Ti(OBu)<sub>4</sub>], Ethanol [CH<sub>3</sub>CH<sub>2</sub>OH], Citric acid [C<sub>6</sub>H<sub>8</sub>O<sub>7</sub>] and Calcium Nitrate [Ca(NO<sub>3</sub>)<sub>2</sub>.4H<sub>2</sub>O] were purchased from Sigma-Aldrich and used without any further purification. Calcium titanate (CaTiO<sub>3</sub>) samples of different molarity (0.1M, 0.3M, 0.5M, 0.7M and 0.9M) were synthesized by using sol-gel technique. A stoichiometric ratios of tetra-butyl titanate [Ti(OBu)<sub>4</sub>], ethanol [CH<sub>3</sub>CH<sub>2</sub>OH], citric acid [C<sub>6</sub>H<sub>8</sub>O<sub>7</sub>] and calcium nitrate [Ca(NO<sub>3</sub>)<sub>2</sub>.4H<sub>2</sub>O] were measured in beaker by AND, BM-22 microgram balance [8]. Firstly, tetra-butyl titanate added drop wise into ethanol under vigorous stirring, the pale yellow ethanol was turned into limethen citric acid is added into the ethanol solution as a chelating agent. So lime solution turned into transparent solution. Afterwards for 1:1 ratio of Ca and Ti we add calcium nitrate. The prepared solutions were poured into a large beaker, and then placed on hot plate with magnetic stirrer at 50°C for 1.5h. Next is drying step, in this step the sol is poured into crucibles and heat at 80°C for 12h in muffle furnace. After drying, xerogel is formed. This xerogel is converted into fine powder with the help of mortar and pestle for the formation of pallets. Apex Hydraulic press was used for pallets formation by applying force of 40 kN for 1min.

For structural analysis Rigaku D Max/II-A with Cuka ( $\lambda=1.5405\text{\AA}$ ) and nickel filter was utilized. The dielectric behavior of prepared samples was investigated by Wayne Kerr 6500B precision impedance analyzer at room temperature in frequency range of 20Hz-20MHz.

## III. RESULT AND DISCUSSIONS

Figure 1(a) Shows the XRD pattern of CaTiO<sub>3</sub>(0.1M-0.9M) samples synthesized by sol-gel method. All the observed peaks located at 25°, 25.8°, 29°, 32°, 39°, 41°, 62.5° and 63° were indexed corresponding to Miller's indices (110), (111), (111), (200), (031), (131), (142) and (051) respectively according to JCPDS # 22-153 of calcium titanate (orthorhombic) [27]. In XRD pattern the highest peak is located at  $2\theta = 25^\circ$  indicates that diffraction which takes place from this plane (110) shows greater concentration of lattice atoms. The well matched peaks of all the calcium titanate (CaTiO<sub>3</sub>) samples (0.1M-0.9M) were not altered, revealing the formation of single (orthorhombic) phase in all samples with good stability. It is noticed that change in molarity has significant role on crystalline nature. The average crystallite size has been calculated from the highest peak using Scherrer's formula. Figure 1(b) indicates that on increasing the molar concentration (0.1M-0.9M), the crystallite size increases gradually upto 0.9M (35nm) and similarly the crystallite size has inverse relation with dislocation density. On increasing the molar concentration the dislocation density decreases which can be explained on the basis of lattice defects. As the crystallite size increases, the contribution of defect decreases. The FWHM reduced and sharp peaks were achieved at higher molarities which offer ascent to increase in crystallinity of samples. Dislocation density has maximum value for 0.1M sample and has lowest values for 0.9M calcium titanate sample. Dislocations arise in calcium titanate samples due to existence of grain boundaries. The polymerization of colloidal particles is mostly done in sol-gel process. The polymerization increases as molar concentration is increased. The increase in molarity gives rise to increase electrostatic interactions between the particles. Hence the chances of collision increases which result in the formation of larger crystallites.

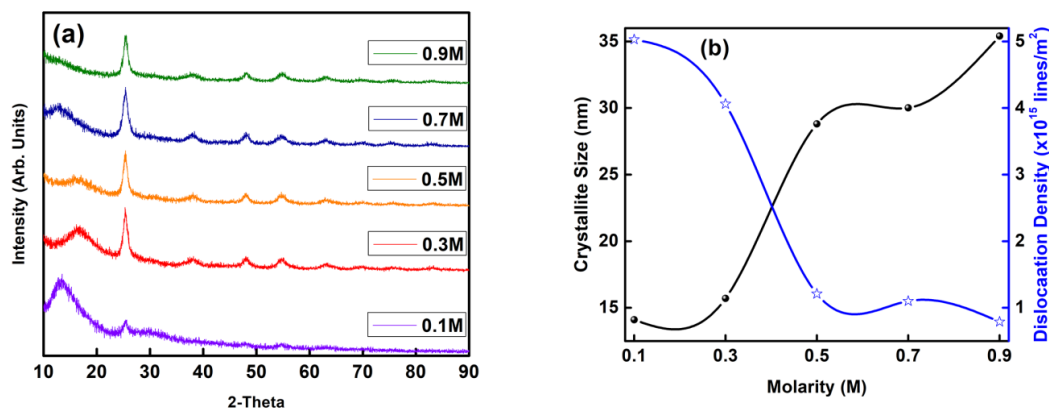


Figure 1: (a) XRD patterns of calcium titanate samples with variation in molarity as ( $x = 0.1M, 0.3M, 0.5M, 0.7M$  and  $0.9M$ ). (b) Crystallite size and dislocation density plotted as a function of molar concentration.

Figure 2 (a) indicates room temperature dielectric constant versus frequency in range of 20 Hz to 20 MHz. It is indicated that value of dielectric constant is maximum for all the samples of calcium titanate for different molarities (0.1M, 0.3M, 0.5M, 0.7M and 0.9M) at lower frequencies and decreases gradually at higher frequencies to show a constant region of dielectric permittivity. The decreasing behavior of real part of dielectric constant at higher frequency ascribed to relaxation phenomena [28, 29]. At low frequency, when an electric field is applied, the dielectric constant is produced due to contribution of all types of polarization mechanisms such as ionic, electronic, dipolar and space charge. All polarization mechanisms have their own relaxation time. Thus shows higher value of the dielectric constant. When frequency increases, the value of dielectric constant decreases due to decreasing contribution of space charge and dipolar polarization [30]. This difference of dielectric permittivity with frequency can be described by Maxwell-Wagner (M-W) model for interfacial or space charge polarization with Koop's phenomenological theory. According to M-W model, that dielectric material is made up of two layers, less resistive layer (grains) and more resistive layer (grain boundaries). Due to charge accumulation at grain boundaries, Maxwell-Wagner interfacial polarization arises. At low-frequency region, the charge carriers follow the applied field due to enough time to align in the direction of field [31]. However, the decrease in dielectric constant with increase in frequency is based on fact that charge carriers  $Ti^{4+} + e^- \leftrightarrow Ti^{3+}$  are unable to follow the field reversal. That's why the value of dielectric constant decreases at higher frequency. Since our system has perovskite structure, where oxygen vacancies are responsible for the production of charge carriers which can take part in conduction phenomena [32]. The phenomena of polarization in titanates ascribed to distortion of  $TiO_6$  octahedron [33]. Thus the hopping of charge exists in channel-like  $Ti^{3+}-O-Ti^{4+}$ . This channel plays a determinate role in conduction process. The value of dielectric constant increases with molarity ascribed to the reduction in imperfections produced due to titanium ion volatilization or oxygen vacancy actions [34]. The increase in dielectric constant with molarity also attributed to larger ionic radius of  $Ti^{3+}$  ( $0.670\text{\AA}$ ) as compared to  $Ti^{4+}$  ( $0.605\text{\AA}$ ) which changes the structural properties due to hopping of  $Ti^{3+}$  into  $Ti^{4+}$  [35].

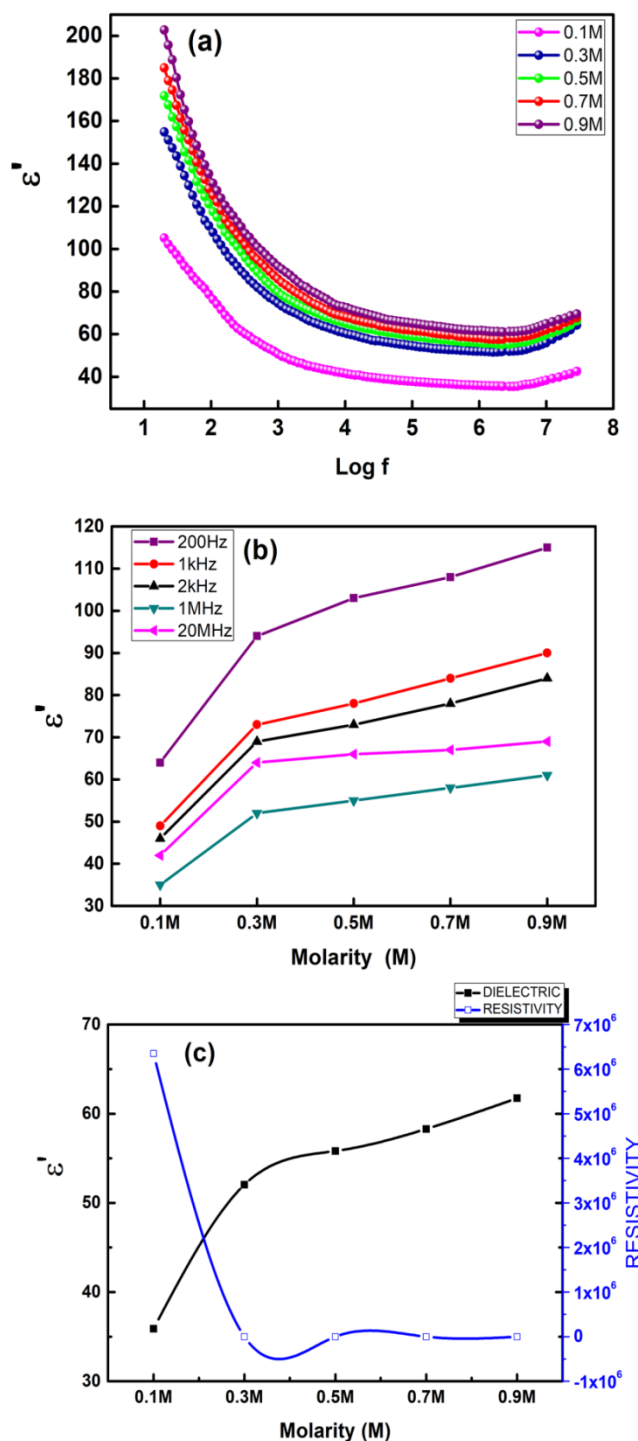


Figure 2: (a) Frequency dependence of dielectric constant ( $\epsilon'$ ) for calcium titanate samples with variation in molarity as ( $x = 0.1M$ ,  $0.3M$ ,  $0.5M$ ,  $0.7M$  and  $0.9M$ ) at RT. (b) Molarity dependent variation of dielectric constant ( $\epsilon'$ ) of calcium titanate samples at different frequencies. (c) Dielectric constant and resistivity plotted as a function of molar concentration.

Figure 2(b) shows the behaviour of real dielectric constant versus molarity. The compensation mechanisms like electric, B-site and oxygen vacancy can be tailor by increasing molar concentration [36]. The variation of real dielectric constant can be credited to variation of grain size because when grain size increases then dielectric constant also increases [37]. The highest value of dielectric constant was shown by 0.9M calcium titanate sample contains largest grain size. This conduct emerges because of increasing involvement of dipolar alignment which is attributed due to the movement of free charge carriers and their nearby dislocations [28]. Figure 2(c) shows comparison between increasing trend of dielectric constant and resistivity with molarity. The increase in dielectric constant with molarity attributed to decrease in resistivity.

Figure 3(a-c) indicate that both imaginary dielectric constant and tangent loss depicted the same behavior as  $\epsilon'$ . The typical decreasing behavior on increasing frequency explained on the basis M-W model. The grains are more energetic at high frequency whereas the grain boundaries become energetic at low frequency. Thus energy losses are high at low frequency due to resistive behavior of grain boundaries which are ascribed with the crystal defects and impurities. At low frequency, charge carriers required high energy for hopping phenomena. In high-frequency region, low resistive grains are active which show the decreasing trend of dielectric loss. The dielectric tangent loss can also be explained on the basis of hopping frequency, when applied frequency is higher than hopping frequency. Low loss has been observed because atoms have enough energy for hopping mechanism [29, 31]. The value of tangent loss strongly depends on homogeneity, imperfections; stoichiometry inside a material, oxygen vacancy generates defects and impurities which cause dielectric losses [38]. The tangent loss value increases with molarity. This behavior attributed to increasing trend of conductivity which also supports the increasing  $\epsilon'$  with molarity [33]. When the molar concentration increases to 0.9M, strong loss peak is observed and this peak shifts towards the lower frequency indicating the reduction of defects and imperfections which leads to strengthen the grain size [28].

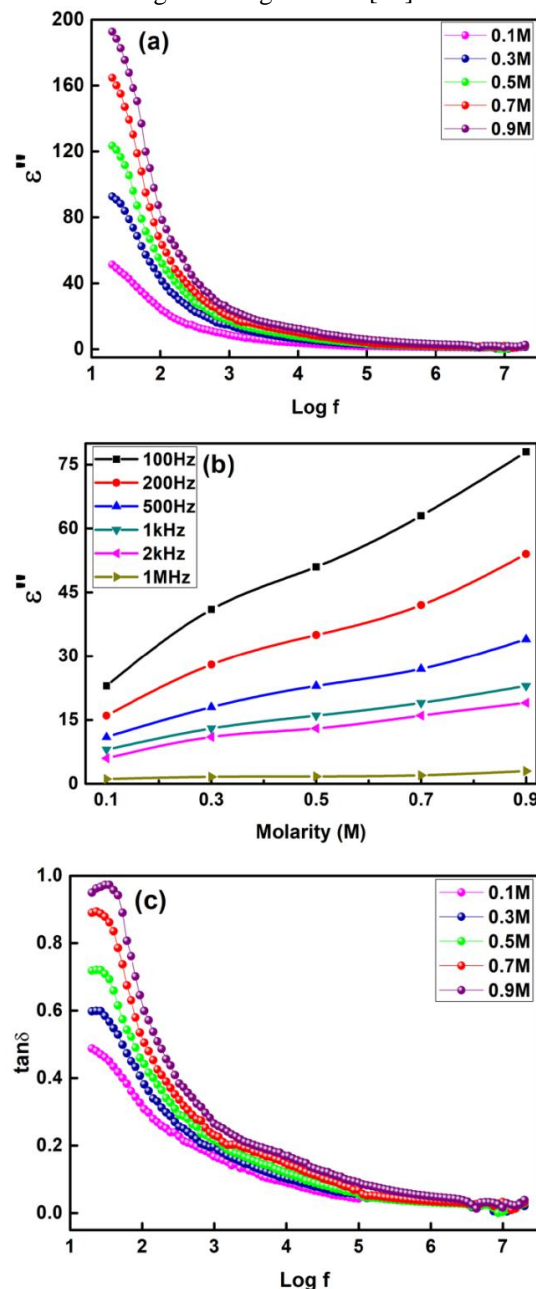


Figure 3: (a) Frequency dependence of dielectric loss ( $\epsilon''$ ) for calcium titanate samples with variation in molarity as ( $x = 0.1M, 0.3M, 0.5M, 0.7M$  and  $0.9M$ ) at RT. (b) Molarity dependent variation of dielectric loss ( $\epsilon''$ ) of calcium titanate samples at different frequencies. (c) Frequency dependence of tangent loss ( $\tan \delta$ ) for calcium titanate samples with variation in molarity as ( $x = 0.1M, 0.3M, 0.5M, 0.7M$  and  $0.9M$ ) at RT.

Figure 4 (a) indicates the AC conductivity of calcium titanate ( $\text{CaTiO}_3$ ) of different molar concentrations (0.1M, 0.3M, 0.5M, 0.7M and 0.9M) at room temperature. The plot revealed that conductivity strongly depends on increasing and decreasing function of frequency. At high frequency hopping of charge carrier increases due to active behavior of grains while at low frequency hopping of charge carriers is minimum due to effective grain boundaries [38, 39]. Further at low frequency, charge carriers jump from one site to another neighboring site which results in conductivity named as long-range transport of charge carriers under the applied field while at higher frequency charge carriers like finite bunches take part in conduction mechanism by hopping [34]. The samples showed two regions of conductivity. The first region from 20Hz-1.5MHz frequency in which conductivity is constant known as frequency independent conductivity ( $\sigma_{dc}$  dc-conductivity) shows frequency exponent  $n=0$  [39]. In the second high frequency region conductivity increases exponentially which is attributed as frequency dependent conductivity ( $\sigma_{ac}$ ). The frequency dependent conductivity can be explained by Johnson's universal power law. According to this law, the phenomena of electrical conduction in the material takes place by hopping of charge carrier from its original position to another position.

$$\sigma_{ac}(\omega) = \sigma_{dc} + A\omega^n$$

where  $\sigma_{dc}$  describes the frequency independent behavior attributed to electronic or dc-conductivity,  $A\omega^n$  shows the AC conductivity, where 'A' is constant indicating amplitude which controls the polarization mechanism and 'n' is the frequency exponent lies in range of  $1 < n < 0$  shows the relation of charge carriers with crystal lattice and  $\omega$  is angular frequency. Hence at higher frequency  $\sigma_{ac}$  strongly related with ' $\omega^n$ '. In perovskite framework the significant method of charge transport is a numerous hopping process. This hopping mechanism regularly happens over the potential obstructions set up by the cross-section structure and the nearby condition of different atoms/ions [11]. Oxygen vacancies in ferroelectric perovskite material play a vibrant role for high conduction in grains [32]. In material, oxygen vacancies liberate conducting electrons which are captured by  $\text{Ti}^{4+}$  to form conductive  $\text{Ti}^{3+}$  ions. The  $\text{Ti}^{4+}$  and  $\text{Ti}^{3+}$  form bonds like  $\text{Ti}^{3+}-\text{O}-\text{Ti}^{4+}$  bonds. The distortion produced in lattice when Ti-3d electrons in  $\text{Ti}^{3+}$  ions can hop to  $\text{Ti}^{4+}$  under external field because ionic radius (0.605Å) of  $\text{Ti}^{4+}$  is smaller than (0.670 Å) of  $\text{Ti}^{3+}$ . Thus the formation of  $\text{Ti}^{3+}$  ions will distort the lattice because of ionic radii difference and produce a polaronic distortion [40,41]. The AC conductivity strongly depend upon hopping of electrons between  $\text{Ti}^{4+}$  and  $\text{Ti}^{3+}$  ions at the octahedral sites. The hopping mechanism increases with frequency which leads to increase in AC conductivity due to charge carrier hopping in finite  $\text{TiO}_6$  clusters. [39,42]. Figure 4 (b) indicates that AC conductivity increases with molarity, which can be ascribed to an increase in charge carriers' drift mobility with increasing molarity. When we increase molarity the electron exchange between  $\text{Ti}^{4+}$  and  $\text{Ti}^{3+}$  ions increases which shows higher conduction mechanism [43]. Figure 4 (c) shows the variation of frequency exponent factor 'n' with molarity. The value of 'n' found by taking slope of conductivity curves. First region of conductivity contains possession of ruse charges. That's why there is no effect of molarity on 'n' values. Whereas second region of conductivity shows increasing trend of exponent 'n' values like 0.385 to 0.802. The increasing values of 'n' in second region attributed to translational hopping of small polarons [31]. As the value of frequency exponent 'n' for different molar concentration samples is less than 1, indicating the non-Debye behavior [32].

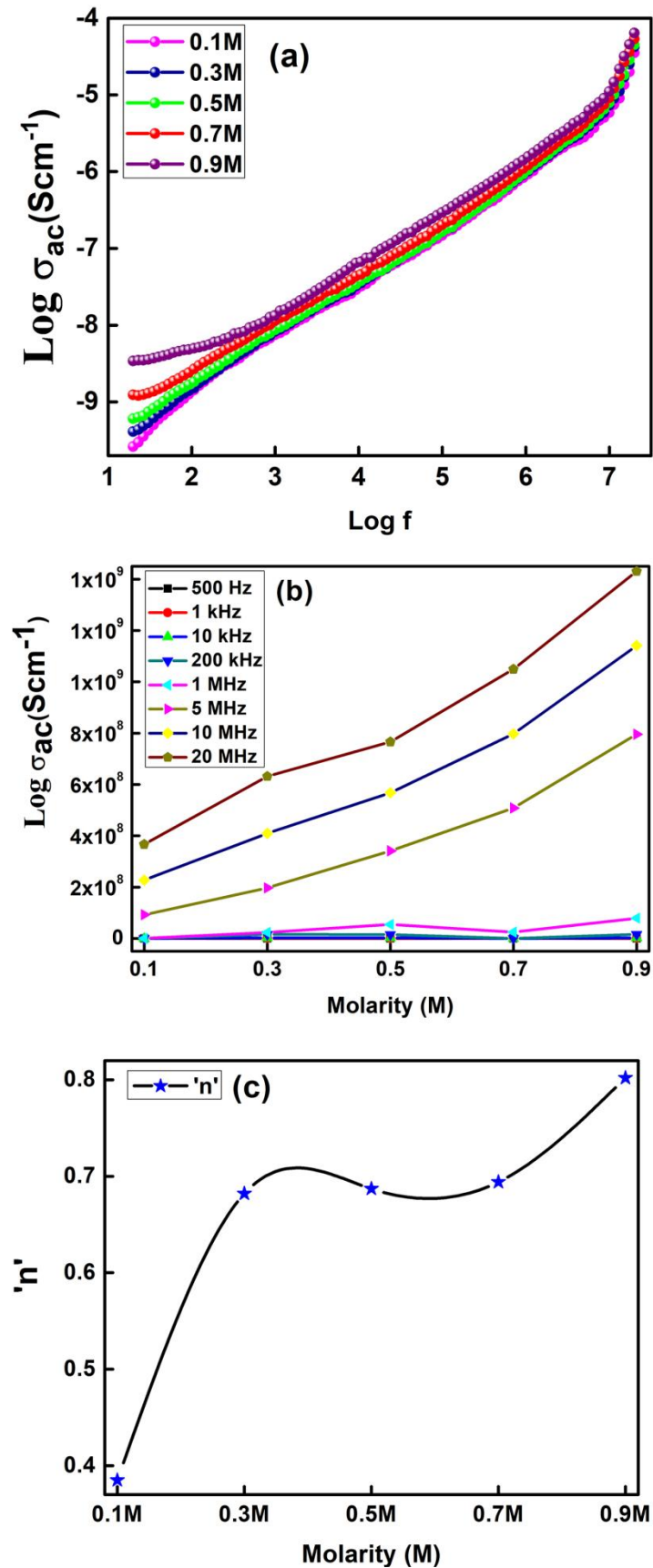


Figure 4: (a) Frequency dependence of ac conductivity for calcium titanate samples with variation in molarity as ( $x = 0.1\text{M}, 0.3\text{M}, 0.5\text{M}, 0.7\text{M}$  and  $0.9\text{M}$ ) at RT.(b)Molarity dependent variation of ac conductivity of calcium titanate samples at different frequencies.(c)Exponent 'n' as a function of molar concentration.

Impedance spectroscopy is used to study the micro structural information in order to separate different contribution of grain, grain boundaries, electrode effect present in the material. The presence of different semicircles intimate that different relaxation time exists. Figure 5 (a) and 5 (b) indicate the variation of real and imaginary parts of impedance. The real part of impedance ( $Z'$ ) exhibits higher values of resistivity. The imaginary part of impedance ( $Z''$ ) shows low values of impedance. Figure 5 (a) indicates that magnitude of  $Z'$  increases at low frequency due to effective grain boundaries while the decreasing behavior of  $Z'$  exhibited at higher frequency due to active grains. When we increase molarity the conductivity of samples increase due to strengthen grain that's why the magnitude of  $Z'$  decreases on increasing molarity. It has been observed the value of  $Z'$  for all calcium titanate samples merged at higher frequency. This effect produces due to release of space charges in material which results in decrease of barrier properties [29, 34, 44]. Figure 5 (b) shows that  $Z''$  values reach a maxima peak for the 0.1M calcium titanate sample. When molarity increases the values of  $Z''$  moves to higher frequencies indicating the rising behavior of capacitance and decreasing values of resistance [34]. Similarly an irregular peak expansion has been observed with the rise in molarity. At low frequency, imaginary plot shows wide and irregular peaks. These peaks describe the Debye behavior because of multiple relaxations. The relaxation process has been arise due to presence of immobile species at lower molar concentration In imaginary part of impedance the effect of broadening peak has been observed due to spread of relaxation time. When space charges assembled in the material, the imaginary impedance values merged at high frequencies. Since peak height is decreased with molarity. The overall impedance decreases with increasing molar concentration [45].

To differentiate between the resistance of grains and grain boundaries Nyquist plot of calcium titanate samples of different molarities (0.1M, 0.3M, 0.5M, 0.7M, 0.9M) at room temperature are displayed in Figure 5 (c). The impedance spectrum obtained by plotting the imaginary  $Z''$  impedance against real  $Z'$  impedance called a Nyquist plot. Nyquist plots are useful to determine the resistance of grains, grain boundaries and relaxation time. Nyquist plot are generally composed of three semicircles. These semi-circles with different radius of curvature matches to resistance of grain boundaries within the sample due to less concentrations of structural and chemical defects. The charge carriers relax at high frequencies while semicircle with large radius shows the resistance of grain boundaries as there is high densities of structural and chemical defects within the grain boundaries and the charge carriers relax at low frequencies. The semicircle arises at low frequency shows the effect of grain boundaries because of high resistance values while the semicircle arises at higher frequency shows the behavior of grains. The third semicircle was also arises in some materials which lie in between the higher and lower frequency which might be attributed to surface effect [46].

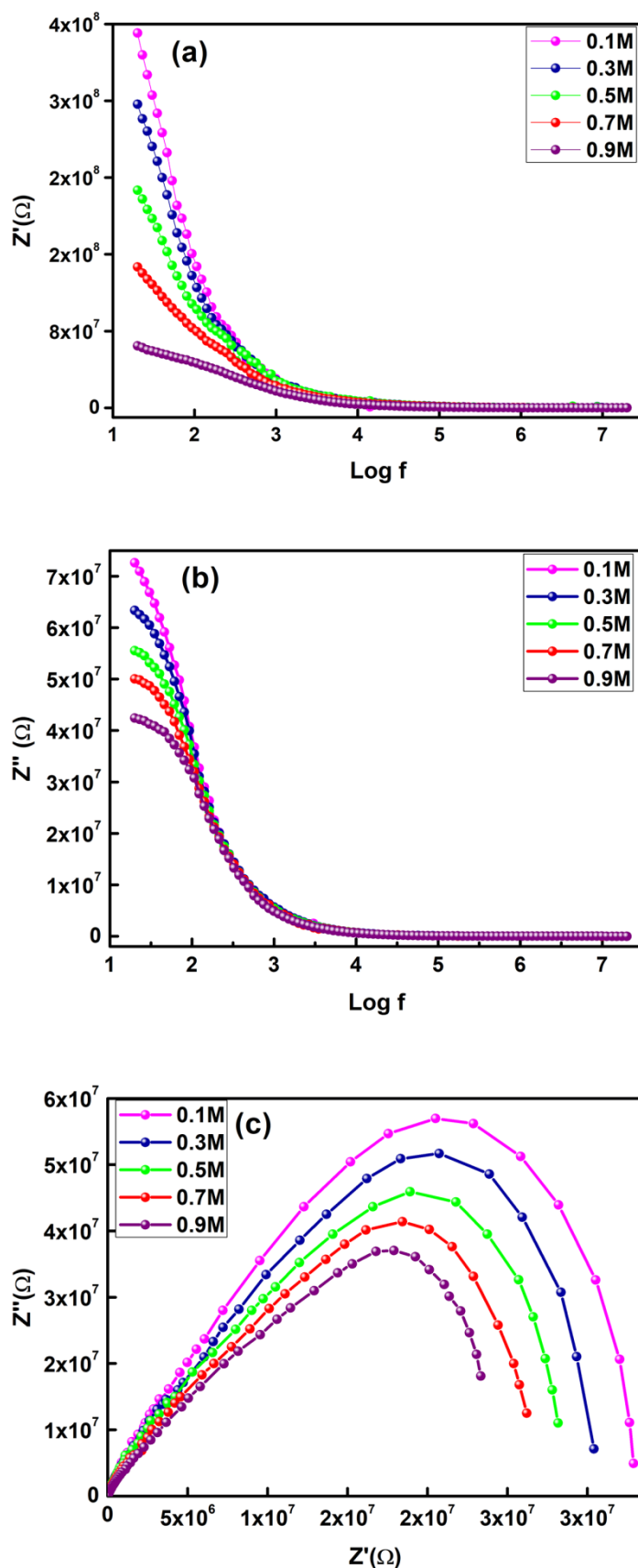


Figure 5: Variation of (a) real part of impedance ( $Z'$ ) and (b) imaginary part of impedance ( $Z''$ ) with frequency of calcium titanate samples ( $x = 0.1M, 0.3M, 0.5M, 0.7M$  and  $0.9M$ ). (c) Complex impedance spectra of calcium titanate samples ( $x = 0.1M, 0.3M, 0.5M, 0.7M$  and  $0.9M$ ) at RT.

In the present work, Nyquist plot for  $\text{CaTiO}_3$  samples with varied molarity (0.1M, 0.3M, 0.5M, 0.7M and 0.9M) have been studied. Figure 5 (c) demonstrates impedance spectra with different semi circles with different radius of curvature due to grain boundary effect. The single semicircular arcs in plot confirm the charge transport phenomena occur due to grains [36]. The sample with 0.9M has lowest value of relaxation time and impedance which can be correlated with dielectric constant. Because this 0.9M sample of calcium titanate has maximum dielectric constant so its dipoles show maximum polarization in short time. The figure shows that the diameter of semicircle decreases on increasing the molar concentration, showing that resistance of grain boundaries and relaxation time is decreasing [29, 34, 46]. Figure 5 (c) indicates that radius of semicircle decreases on increase molarity. The curve shift towards the real part of impedance which indicates the increasing trend of conductivity and at lower molar concentration where diameter of semicircle is large i.e. 0.1M, 0.3M and 0.5M the contribution of grain boundaries is high as compare to grains but on further increase in molarity the contribution of grains increase as compare to grain boundaries where diameter of semicircle start to decrease. When molar concentration increases, the peaks of imaginary part moves to higher frequency and the intensity of peak also decreases. This behavior indicates that contribution of grain boundaries start to decrease with increase in molarity [47]. The data also indicate the existence of one semicircle, representing the single type of relaxation phenomena at different relaxation time ( $\tau=RC$ ), as observed for calcium titanate ( $x=0.1M, 0.3M, 0.5M, 0.7M$  and  $0.9M$ ) samples at RT. The contribution of grains, grain boundaries and surface effect are also shown separately by theoretical modeling of the data into equivalent circuit, consisting of R-C (resistor-capacitor) parallel combination. The values of  $R_{gb}$  for grain boundaries are calculated from the peak of circular arc intercepts on  $Z'$  axis while the capacitive components  $C_{gb}$  are calculated from relation  $\omega_{max}RC=1$  (where  $\omega_{max}$  is the maximum value of frequency at  $Z''$  axis) [48]. By using this relation, the relaxation time  $\tau_{gb}$  for grain boundaries are also calculated and listed in Table: 1. The center of semicircle lies below real impedance axis indicating the non-Debye type behavior. The Table: 1 shows that grain boundary resistance decreases on increasing molar concentration. This effect is attributed to increasing contribution of charge carriers towards conduction mechanism. The decreasing trend of grain boundary resistance with molarity is shown in table [34].

**Table 1: Impedance parameters obtained from grains and grain boundaries of calcium titanate samples with variation in molarity as ( $x = 0.1M, 0.3M, 0.5M, 0.7M$  and  $0.9M$ ) at RT.**

Conc.	$R_{gb}(k\Omega)$	$C_{gb}(pF)$	$\tau_{gb}(\mu s)$	$\omega_{gb}$
0.1	$2.28 \times 10^7$	$5.37 \times 10^{10}$	$1.22 \times 10^{18}$	8164
0.3	$2.07 \times 10^7$	$5.15 \times 10^{10}$	$1.06 \times 10^{18}$	9420
0.5	$1.89 \times 10^7$	$4.21 \times 10^{10}$	$7.95 \times 10^{17}$	12560
0.7	$1.61 \times 10^7$	$4.31 \times 10^{10}$	$6.93 \times 10^{17}$	14444
0.9	$1.52 \times 10^7$	$3.89 \times 10^{10}$	$5.91 \times 10^{17}$	16956

#### IV. CONCLUSION

Single phase Calcium Titanate ceramics of different molarities ( $x= 0.1M, 0.3M, 0.5M, 0.7M$  and  $0.9M$ ) were prepared by sol-gel method. XRD pattern showed pure orthorhombic phase of  $\text{CaTiO}_3$  in all molarities upto  $0.9M$ , whereas, increase in crystallinity was observed with the increase of molarity. Dielectric constant as a function of frequency increased exponentially with increase of molar concentration up to  $0.9M$  attributed to high density and large crystallite size. The dielectric constant of all samples showed the Maxwell-Wagner interfacial and dipolar polarization with agreement of Koop's phenomenological theory. The dielectric loss showed the same trend as dielectric constant indicates increasing behavior of conductivity with molarity. The increase in AC conductivity with molar concentration has been explained on the basis of electronic exchange phenomena. This phenomenon arises due to formation of  $\text{Ti}^{3+}$  ions due to partial reduction of  $\text{Ti}^{4+}$  ions. The variation of frequency exponent 's' values (0.385 to 0.802) showed that conduction mechanism arises due to small polaron hopping. Impedance analysis showed one semicircle, which explains the behavior of grain boundaries. The diameter of semicircle decreases on increasing molarity which showed that resistance of grain boundaries and relaxation time is decreasing. In conclusion, ceramics synthesized by such variation of molarity without thermal annealing evidenced to be successful to improve dielectric properties which are fundamental for capacitive applications.

**Funding**

The work is supported by the Higher Education Commission of Pakistan start-up research [grants No: 21-2344/SRGP/R&D/HEC/2019 and 21-2340/SRGP/R&D/HEC/2019].

**REFERENCES**

- [1]. Aziz, A., Ahmed, E., Ashiq, M. N., Ehsan, M. F., Ali, I., & Khan, M. A. (2016). Role of Ni-Co co-substitution in improving electrical and dielectric properties of La-based multiferroic nanomaterials. *Ceramics International*, 42(4), 5218-5225.
- [2]. Liu, Y., Wang, W., Huang, J., Tang, F., Zhu, C., & Cao, Y. (2013). Dielectric properties of giant permittivity  $\text{NaCu}_3\text{Ti}_3\text{NbO}_{12}$  ceramics. *Ceramics International*, 39(8), 9201-9206.
- [3]. Demirors, A. F., & Imhof, A. (2009).  $\text{BaTiO}_3$ ,  $\text{SrTiO}_3$ ,  $\text{CaTiO}_3$ , and  $\text{Ba}_x\text{Sr}_{1-x}\text{TiO}_3$  Particles: A General Approach for Monodisperse Colloidal Perovskites. *Chemistry of Materials*, 21(13), 3002-3007.
- [4]. Wang, L., Li, J., Feng, M., Min, L., Yang, J., Yu, S., & Yang, Z. (2017). Perovskite-type calcium titanate nanoparticles as novel matrix for designing sensitive electrochemical biosensing. *Biosensors and Bioelectronics*, 96, 220-226.
- [5]. Han, C., Liu, J., Yang, W., Wu, Q., Yang, H., & Xue, X. (2016). Enhancement of photocatalytic activity of  $\text{CaTiO}_3$  through  $\text{HNO}_3$  acidification. *Journal of Photochemistry and Photobiology A: Chemistry*, 322, 1-9.
- [6]. Hosseini, N. R., Sammes, N. M., & Chung, J. S. (2014). Manganese-doped lanthanum calcium titanate as an interconnect for flat-tubular solid oxide fuel cells. *Journal of Power Sources*, 245, 599-608.
- [7]. Sindhu, M., Ahlawat, N., Sanghi, S., Agarwal, A., Dahiya, R., & Ahlawat, N. (2012). Rietveld refinement and impedance spectroscopy of calcium titanate. *Current Applied Physics*, 12(6), 1429-1435.
- [8]. Han, C., Liu, J., Yang, W., Wu, Q., Yang, H., & Xue, X. (2017). Photocatalytic activity of  $\text{CaTiO}_3$  synthesized by solid state, sol-gel and hydrothermal methods. *Journal of Sol-Gel Science and Technology*, 81(3), 806-813.
- [9]. Gargori, C., Cerro, S., Galindo, R., García, A., Llusar, M., Badenes, J., & Monrós, G. (2011). New vanadium doped calcium titanate ceramic pigment. *Ceramics International*, 37(8), 3665-3670.
- [10]. Chong, H. A. N., He, Y. A. N. G., & XUE, X. X. (2014). Effects of Fe content on photocatalytic activity of  $\text{CaTiO}_3\text{-Fe}_x$ . *Transactions of Nonferrous Metals Society of China*, 24(10), 3215-3220.
- [11]. Rafiq, M. A., Rafiq, M. N., & Saravanan, K. V. (2015). Dielectric and impedance spectroscopic studies of lead-free barium- calcium- zirconium- titanium oxide ceramics. *Ceramics International*, 41(9), 11436-11444.
- [12]. Afghahi, S. S. S., Jafarian, M., Zargari, S., & Atassi, Y. (2017). Synthesis of Calcium Titanate Powder with Hollow Square Based Prism Morphology via One-Step Surfactant-Free Hydrothermal Method: Temperature Effect and Optical Properties. *Transactions of the Indian Ceramic Society*, 76(4), 237-241.
- [13]. Cesconeto, F. R., Borlaug, M., Nieto, M. I., de Oliveira, A. P. N., & Moreno, R. (2018). Synthesis of  $\text{CaTiO}_3$  and  $\text{CaTiO}_3/\text{TiO}_2$  nanoparticle compounds through  $\text{Ca}^{+2}/\text{TiO}_2$  colloidal sols: Structural and photocatalytic characterization. *Ceramics International*, 44(1), 301-309.
- [14]. Gaikwad, S. S., Borhade, A. V., & Gaikwad, V. B. (2012). A green chemistry approach for synthesis of  $\text{CaTiO}_3$  Photocatalyst: its effects on degradation of methylene blue, phytotoxicity and microbial Study. *Der PharmaChemica*, 4, 184-193.
- [15]. Durrani, S. K., Khan, Y., Ahmed, N., Ahmad, M., & Hussain, M. A. (2011). Hydrothermal growth of calcium titanate nanowires from titania. *Journal of the Iranian Chemical Society*, 8(2), 562-569.
- [16]. Hosseini, S. A. (2017). Preparation and characterization of calcium titanate nanoparticles with the aid of different acids and study of their photocatalytic properties. *Journal of Materials Science: Materials in Electronics*, 28(4), 3703-3708.
- [17]. Wong, Y. J., Hassan, J., & Hashim, M. (2013). Dielectric properties, impedance analysis and modulus behaviour of  $\text{CaTiO}_3$  ceramic prepared by solid-state reaction. *Journal of Alloys and Compounds*, 571, 138-144.
- [18]. Ctibor, P., Kotlan, J., Pala, Z., Sedlacek, J., Hajkova, Z., & Grygar, T. M. (2015). Calcium titanate ( $\text{CaTiO}_3$ ) dielectrics prepared by plasma spray and post-deposition thermal treatment. *Materials Research Bulletin*, 72, 123-132.
- [19]. Dong, W., Song, B., Meng, W., Zhao, G., & Han, G. (2015). A simple solvothermal process to synthesize  $\text{CaTiO}_3$  microspheres and its photocatalytic properties. *Applied Surface Science*, 349, 272-278.
- [20]. H. Zhao, Y. Duan, X. Sun, Synthesis and characterization of  $\text{CaTiO}_3$  particles with controlled shape and size, *New J. Chem.* 37 (2013) 986–991.
- [21]. C. Sun, K.N. Sun, *Phys. B: Condens. Matter* 391 (2007) 335–338.
- [22]. M. Muthuraman, K.C. Patil, S. Senbagaraman, A.M. Umarji, *Mater. Res. Bull.* 31 (1996) 1375–1381
- [23]. Y. Pan, Q. Su, H. Xu, T. Chen, W. Ge, C. Yang, M. Wu, *J. Solid State Chem.* 174 (1) (2003) 69–73
- [24]. S.J. Lee, Y.C. Kim, J.H. Hwang, *J. Ceram. Process. Res.* 5 (2004) 223–226.
- [25]. Mohammadi, M. R., & Fray, D. J. (2013). Synthesis of highly pure nanocrystalline and mesoporous  $\text{CaTiO}_3$  by a particulate sol-gel route at the low temperature. *Journal of sol-gel science and technology*, 68(2), 324-333.
- [26]. C. J. Brinker and G. W. Scherer, *Sol-Gel Science—The Physics and Chemistry of Sol-Gel Processes*. New York, NY, USA: Academic, 1990.
- [27]. Li, Q., Yan, R., Dong, L. M., & Zhang, Y. F. (2017). ELECTROSPINNING PREPARATION AND LUMINESCENCE PROPERTIES OF  $\text{CaTiO}_3\text{:RE (Eu}^{3+}/\text{Gd}^{3+})$  NANOFIBERS. *Digest Journal of Nanomaterials&Biostructures (DJNB)*, 12(1).
- [28]. Mustafa, G. M., Atiq, S., Abbas, S. K., Riaz, S., & Naseem, S. (2018). Tunable structural and electrical impedance properties of pyrochlores based Nd doped lanthanum zirconate nanoparticles for capacitive applications. *Ceramics International*, 44(2), 2170-2177.
- [29]. Purohit, V., Padhee, R., & Choudhary, R. N. P. (2018). Dielectric and impedance spectroscopy of  $\text{Bi (Ca}_{0.5}\text{Ti}_{0.5})\text{O}_3$  ceramic. *Ceramics International*, 44(4), 3993-3999.
- [30]. Sarangi, S., Badapanda, T., Behera, B., & Anwar, S. (2013). Frequency and temperature dependence dielectric behaviour of barium zirconatetitanatenanocrystalline powder obtained by mechanochemical synthesis. *Journal of Materials Science: Materials in Electronics*, 24(10), 4033-4042
- [31]. Atiq, S., Majeed, M., Ahmad, A., Abbas, S. K., Saleem, M., Riaz, S., & Naseem, S. (2017). Synthesis and investigation of structural, morphological, magnetic, dielectric and impedance spectroscopic characteristics of Ni-Zn ferrite nanoparticles. *Ceramics International*, 43(2), 2486-2494.
- [32]. Rani, S., Ahlawat, N., Punia, R., Sangwan, K. M., & Rani, S. (2018). Dielectric relaxation and conduction mechanism of complex perovskite  $\text{Ca}_{0.90}\text{Sr}_{0.10}\text{Cu}_3\text{Ti}_3.95\text{Zn}_{0.05}\text{O}_{12}$  ceramic. *Ceramics International*, 44(6), 5996-6001.
- [33]. Singh, J. P., Gautam, S., Kumar, P., Tripathi, A., Chen, J. M., Chae, K. H., & Asokan, K. (2013). Correlation between the dielectric properties and local electronic structure of copper doped calcium titanate. *Journal of Alloys and Compounds*, 572, 84-89.

- [34]. Subohi, O., Bowen, C. R., Malik, M. M., &Kurchania, R. (2016). Dielectric spectroscopy and ferroelectric properties of magnesium modified bismuth titanate ceramics. *Journal of Alloys and Compounds*, 688, 27-36.
- [35]. Mustafa, G. M., Saleem, M., Atiq, S., Riaz, S., Siddiqi, S. A., &Naseem, S. (2018). Structural Tuning of Dielectric Properties of Ce-substituted  $\text{Nd}_2\text{Zr}_2\text{O}_7$ . *Journal of Saudi Chemical Society*.
- [36]. Narang, S. B., Kaur, D., &Pubby, K. (2015). Dielectric and Impedance Spectroscopy of Samarium and Lanthanum Doped Barium Titanate at Room Temperature. *World Academy of Science, Engineering and Technology, International Journal of Environmental, Chemical, Ecological, Geological and Geophysical Engineering*, 9(6), 667-671.
- [37]. Mu, C., Zhang, H., He, Y., & Liu, P. (2010). Influence of temperature on dielectric properties of Fe-doped  $\text{CaCu}_3\text{Ti}_4\text{O}_{12}$  ceramics. *Physica B: Condensed Matter*, 405(1), 386-389.
- [38]. Amin, M., Rafique, H. M., Yousaf, M., Ramay, S. M., &Atiq, S. (2016). Structural and impedance spectroscopic analysis of Sr/Mn modified  $\text{BiFeO}_3$ multiferroics. *Journal of Materials Science: Materials in Electronics*, 27(10), 11003-11011.
- [39]. Karamat, N., Ali, I., Aziz, A., Sher, M., &Ashiq, M. N. (2015). Electrical and dielectric studies of substituted holmium based pyrochlorezirconatesnanomaterials. *Journal of Alloys and Compounds*, 652, 83-90.
- [40]. Zhang, L., & Tang, Z. J. (2004). Polaron relaxation and variable-range-hopping conductivity in the giant-dielectric-constant material  $\text{CaCu}_3\text{Ti}_4\text{O}_{12}$ . *Physical Review B*, 70(17), 174306
- [41]. Zhang, B., Zhao, Q., Chang, A., Ye, H., Chen, S., & Wu, Y. (2014). New negative temperature coefficient thermistor ceramics in Mn-doped  $\text{CaCu}_{3-x}\text{Mn}_x\text{Ti}_4\text{O}_{12}$  ( $0 \leq x \leq 1$ ) system. *Ceramics International*, 40(7), 11221-11227.
- [42]. Mishra, A., Choudhary, S. N., Prasad, K., &Choudhary, R. N. P. (2011). Complex impedance spectroscopic studies of Ba ( $\text{Pr}_{1/2}\text{Ta}_{1/2}$ )  $\text{O}_3$  ceramic. *Physica B: Condensed Matter*, 406(17), 3279-3284.
- [43]. Rostami, Z. A., Ghahfarokhi, S. M., &Kazeminezhad, I. (2018). Effect of Fe/Pb molar ratio on the structure, magnetic and dielectric properties of  $\text{PbFe}_{12}\text{O}_{19}$  nanoparticles. *Chinese journal of physics*, 56(2), 760-769.
- [44]. Chaouchi, A., &Kennour, S. (2012). Impedance spectroscopy studies on lead-free  $(\text{Ba}_{0.85}\text{Ca}_{0.15})(\text{Ti}_{0.9}\text{Zr}_{0.1})\text{O}_3$  ceramics. *Processing and Application of Ceramics*, 6(4), 201-207.
- [45]. Suman, C. K., Prasad, K., &Choudhary, R. N. P. (2005). Impedance spectroscopic studies of ferroelectric  $\text{Pb}_2\text{Sb}_3\text{DyTi}_5\text{O}_{18}$  ceramic. *Advances in applied ceramics*, 104(6), 294-299.
- [46]. Ahmad, Z., Atiq, S., Abbas, S. K., Ramay, S. M., Riaz, S., &Naseem, S. (2016). Structural and complex impedance spectroscopic studies of Mg-substituted  $\text{CoFe}_2\text{O}_4$ . *Ceramics International*, 42(16), 18271-18282.
- [47]. Sangwong, N., Somphan, W., Thongbai, P., Yamwong, T., &Meansiri, S. (2012). Electrical responses and dielectric relaxations in giant permittivity  $\text{NaCu}_3\text{Ti}_3\text{TaO}_{12}$  ceramics. *Applied Physics A*, 108(2), 385-392.
- [48]. Kolekar, Y. D., Sanchez, L., Rubio, E. J., &Ramana, C. V. (2014). Grain and grain boundary effects on the frequency and temperature dependent dielectric properties of cobalt ferrite–hafnium composites. *Solid State Communications*, 184, 34-39.

Dr. Ahmad Hussain, et. al. "Molarity Dependent Structural and Dielectric Behavior of Calcium Titanate Ceramics." *American Journal of Engineering Research (AJER)*, vol. 10(9), 2021, pp. 08-19.